Contract No:

This document was prepared in conjunction with work accomplished under Contract No. 89303321CEM000080 with the U.S. Department of Energy (DOE) Office of Environmental Management (EM).

Disclaimer:

SRNL-STI-2023-00036

Proceedings of the ASME 2023
Pressure Vessels & Piping Conference
PVP2023
July 16-21, 2023, Atlanta, Georgia, USA

PVP2023-106471

ARTIFICIAL NEURAL NETWORKS FOR PREDICTING BURST STRENGTH OF THICK AND THIN-WALLED PRESSURE VESSELS

William R. Johnson, Xian-Kui Zhu, Robert Sindelar, Bruce Wiersma

Savannah River National Laboratory, Aiken SC

ABSTRACT

The common use of pressure vessels (PVs) and linepipes and the high cost of their failure or overdesign in the oil and gas industry makes predicting their burst pressure critical. However, experimental tests of burst pressure are expensive and finite element analysis (FEA) is time consuming. Artificial neural networks (ANNs) hold the promise of rapid prediction of burst strength for a wide range of PV materials and geometries, including pipelines with defects such as corrosion. Here we demonstrate ANNs designed and trained to accurately predict the burst strength of both thick and thin-walled PVs ranging in linepipe steels from X42 to X120. To accomplish this, we trained single and double hidden layer ANNs on experimental augmented with FEA data of predicted burst strength to create a larger database. A statistical study of hundreds of models exploring the key hyperparameters provided statistically optimal hyperparameters, resulting in highly accurate ANNs. The results, two ANNs with comparably low prediction error across geometries ranging from $3 < D_o/t < 120$*, demonstrate the first use of ANNs to address both thick and thin-walled PV burst pressure with a single network. This is an important step towards designing ANNs for predicting the burst strength of PVs and pipelines with defects.*

Keywords: artificial neural network, thick-walled, thin-walled, pressure vessel, linepipe

NOMENCLATURE

P_b	burst pressure
D_o	outer diameter
D_i	inner diameter
σ_y	yield stress
σ_{uts}	engineering ultimate tensile strength
n	strain hardening exponent
C	burst strength model coefficient
x_i	ANN neuron inputs
w_i	ANN weights
b	ANN neuron bias offset
τ	ANN neuron sum
$f(\tau)$	activation function
x_{min}	data minimum value
x_{max}	data maximum value
$y_{n_{pred}}$	algorithm predicted value
$y_{n_{act}}$	data measured value

1. INTRODUCTION

Models for the burst strength of pressure vessels (PVs) and linepipes abound. Law and Bowie, in reference[1], compared 23 different theories for the burst strength of thin-walled PVs and 6 different theories for the burst strain. In reference [2] Christopher et. al. reviewed 12 different burst pressure models for thin and thick-walled PVs. These models tend to fall into categories of either analytically based models derived from first principles or recursive formulas derived from experimental data. Some commonly used analytically derived models include the Barlow formulae [1], the Nadai formulae [3, 4], and the Zhu-Leis formula [5]. Common examples of experimentally derived models include Faupel's [6] and Svennson's [7]. These models, which have varying degrees of effectiveness, tend to have some limitations. If they are experimentally derived, they are often not effective outside of the material or geometric range of data they were developed on. Theoretical models tend to make simplifying assumptions that limit them to only a certain class of PV's, such as thin or thick-walled. Only recently, Zhu et. al. extended the Zhu-Leis PV burst formula for thick walls, providing the first generally applicable theory for both thin and thick-walled power law hardening materials [8].

The PV industry also typically accepts finite element (FE) modeling as a valid technique for predicting PV burst. FE models are often used for damaged or irregular geometries because it is difficult to develop theoretical or empirical models in these cases. For example, references [9] – [13] all used FE modeling to assess the burst pressure of corroded pipelines. References [14] and [15] used FE models to assess the burst strength of irregular geometries. To determine the burst pressure most FE

codes use a RIKS type analysis that assumes the von Mises flow theory of plasticity. Consequently, FE models generally predict the same burst pressure that the von Mises theory predicts. In reference [5] Zhu and Leis developed a mathematical technique to determine, from the FE calculated burst pressure, the Zhu-Leis (average shear stress burst theory), as opposed to von Mises burst pressure, which provides an upper bound on possible burst pressure. Finite element analysis (FEA) has also been used to develop surrogate databases for empirical burst pressure data, as in references [16] and [17], which both developed curve fits to numerically derived PV burst data.

Even though much progress has been made on the analytical modeling of PV burst strength, analytical models fail to capture the scatter in burst pressures that is present in empirically derived data. As noted earlier, it is also difficult to apply analytical models to defects in PVs or pipelines. Artificial neural networks (ANN's) show promise in these directions. Early work on applying ANN's to the PV burst problem looked at predicting the effect of interacting defects on pipe burst pressure [18]. Other work has also looked at using ANNs to predict the burst pressure of defect free pipes [19], the burst pressure of dented pipelines [20], and the use of an adaptive neuro-fuzzy inference system (ANFIS) to predict PV burst pressure from experimental data. ANFIS, a type of ANN that uses fuzzy logic to reduce noise in data, resulted in a high accuracy prediction of PV burst strength [21]. Reference [22] compared ANNs to other types of machine learning such as support vector regression and random forest regression, finding comparable performance. In reference [22] Phan et. al. showed that machine learning algorithms did not effectively predict burst pressure outside of the range of parameters they were trained on, confirming the need for ANN training on a range of data encompassing the parameter range of interest.

In this work we present two different artificial neural networks (ANNs) to predict pressure vessel burst strength over a wide range of material properties and geometric parameters, including both thick and thin walled PVs. The parameters for these ANNs come from experimental data presented in various papers in the literature [23] – [34] previously used by Zhu and Leis to develop and test their average shear stress yield criterion [35] augmented by burst pressure data provided by a finite element model as described in reference [17]. The ANN's include a single hidden layer network, indicated as model 1, and 2 hidden layer network, indicated as model 2. Although deeper ANN's could have also been explored, this has been done in other work for pipelines [20], but seems unnecessary for the relatively small number of input variables needed to model unblemished pipelines. This work explores the hyperparameters of the 1 and 2 layer models to obtain optimal performance as well as compares their performance to known theory predicting PV burst strength.

2. BURST PRESSURE DATABASE DEVELOPMENT

2.1 Experimental Database

Experimental tests of PV burst pressure are expensive, and as a result there is a limited amount of experimental data extant in the literature. A search in the literature has so far found approximately 170 data points for unblemished PVs and pipelines, in references [23] – [34]. Data from these sources cover a wide range of geometric properties, with the outer diameter to thickness ratio (D_o/t) ranging from 3 to 114. All of the experimental data was obtained from strain hardening materials with ultimate tensile strength (UTS) ranging from approximately 49 to 162 ksi and strain hardening exponent n ranging from approximately 0.004 to 0.22. These material properties cover a wide span of linepipe steels, from X42 to X120.

2.2 Numerical Database

FE derived burst pressure further augmented the experimental data to provide a larger dataset for training the ANNs. Reference [17] describes the FE modeling in greater detail. To summarize, a python script generated the PV models and simulated their burst using a static Riks analysis for 60 different cases. These cases include 12 different geometric designs with D_o/t values of 8, 10.67, 16, 21.33, 24, 32, 40, 48, 60, 84, 96, and 120. Each of these geometries was evaluated with 5 different strain hardening pipeline steel models including grade B, X52, X65, X70, and X80. The code used the technique described in [5] to calculate the Zhu-Leis burst pressure from the FE data. The numerical database adopted the Zhu-Leis burst pressure as the actual burst pressure because the average of the von Mises (upper bound) and Tresca (lower bound) theory burst pressures which it supplies is more accurate. Although additional FE PV burst data could be added *ad infinitum*, only these 60 data points were added, to allow the database to contain mostly experimental data. The FE derived PV burst data is included in Appendix A.

2.3 Comparison of Combined Database with Theoretical Solutions

The combined database of 229 points was compared to the analytical thick-walled PV burst equation recently derived in reference [8], given as

$$P_b = 2\left(\frac{C}{2}\right)^{n+1} \sigma_{uts} \ln\left(\frac{D_o}{D_i}\right) \tag{1}$$

where

$$C = \begin{cases} 1 & \text{Tresca Theory} \\ \dfrac{2}{\sqrt{3}} & \text{Von Mises Theory} \\ \dfrac{1}{2} + \dfrac{1}{\sqrt{3}} & \text{Zhu} - \text{Leis Theory} \end{cases} \tag{2}$$

and P_b is the PV burst strength, σ_{uts} is the engineering UTS, D_o is the pipe outer diameter, and D_i is the pipe inner diameter. The

strain hardening exponent n is a function of σ_{uts} and σ_y, found previously to be [36]

$$n = 0.239\left(\frac{\sigma_{uts}}{\sigma_y} - 1\right)^{0.596} \quad (3)$$

Both the experimental and FEA data are plotted in Fig. 1, compared to the Mises, Zhu-Leis, and Tresca analytical theories provided by Eq. (2). The Mises and Tresca solutions give upper and lower bounds to the burst pressure data, respectively, while the Zhu-Leis solution provides an average.

2.4 Feature Selection

Features for ANN training were selected based on their effect on the output variable, in this case the PV burst pressure. The variables considered include D_o, D_o/D_i, the wall thickness t, the yield strength σ_y, the ultimate tensile strength σ_{uts}, and n, due to their known effect on the burst pressure as shown in Eqs. (1) and (3). Figure 2 shows a heat map of the correlation matrix of these variables, calculated as the absolute value of their cross-correlations from their values within the combined database. The figure shows the burst pressure P_b is closely correlated to D_o/D_i, D_o, t, σ_{uts}, and σ_{ys}. For pipe geometries, the theory and curve fitting show that P_b depends only on the diameter ratio D_o/D_i. Within the material properties, as is shown in Eq. (3), only two of the three material parameters σ_{uts}, σ_{ys}, and n are independent, with σ_{uts} and σ_{ys} having a much higher correlation with P_b than n. Consequently, D_o/D_i, σ_{uts}, and σ_{ys} were selected for the ANN.

3. ARTIFICIAL NEURAL NETWORKS

3.1 ANN Architecture

ANNs, a subset of machine learning techniques, attempt to mimic the behavior and connections within biological neural networks (e.g. the human brain) [37]. ANN's are composed of an input layer, a variable number of "hidden" layers, and an output layer. Two examples of interest in this work, a 1-layer and a 2-layer ANN named model 1 and model 2, respectively, are shown in Figs. 3 and 4 respectively.

In an ANN the input layer receives the values for the selected features, each subsequent neuron receives weighted values from the previous layer and performs calculations on that data, and then finally the output layer synthesizes the calculations of the hidden layers to provide the ANN's prediction of PV burst strength. Because this work is interested in predicting PV burst strength, a supervised regressive feedforward network was developed. The weights to this network were updated using the backpropagation algorithm. Sec. **Error! Reference source not found.** describes the feature selection for PV burst.

3.2 Neurons and Activation Functions

Figure 5 shows a typical individual neuron within an ANN network hidden layer. Each neuron receives the inputs x_i from the previous layer, sums the weighted values w_i of these inputs, and adds a bias b to this sum according to

$$\tau = b + \sum_i w_i x_i. \quad (4)$$

The output of the neuron, passed on to subsequent layers in the network, is a function of this value, $f(\tau)$. This function is known as the activation function.

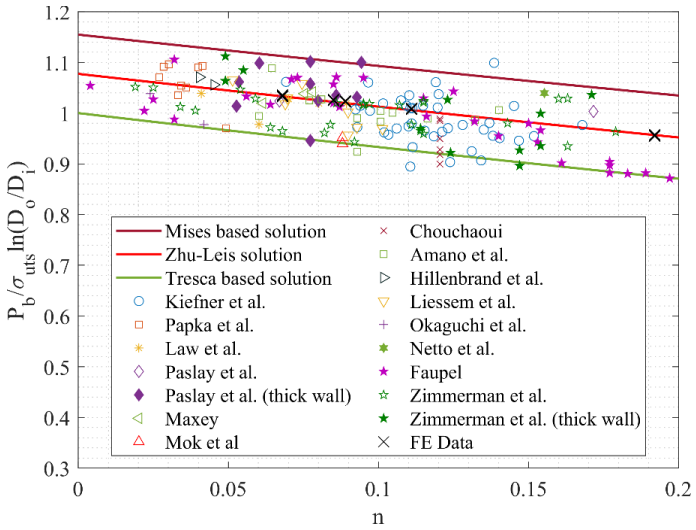

FIGURE 1: PRESSURE VESSEL BURST STRENGTH NORMALIZED USING THE ZHU-LEI'S THICK-WALLED BURST STRENGTH THEORY, WITH FILLED IN MARKERS INDICATING THICK-WALLED CASES ($D_o/t \geq 20$).

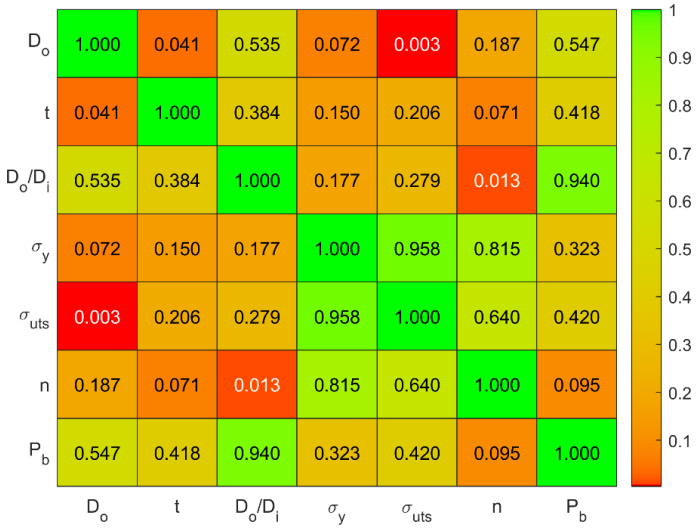

FIGURE 2: CORRELATION MATRIX USED FOR FEATURE SELECTION OF PARAMETERS FOR ANN, WITH VALUES GIVEN AS THE ABSOLUTE VALUE OF THE COHERENCE BETWEEN PARAMETERS.

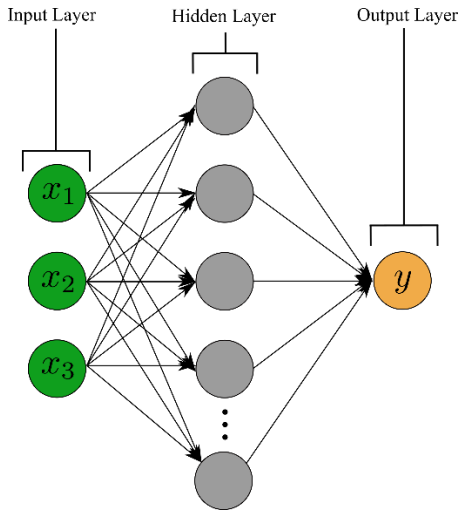

FIGURE 3: THE 1-LAYER ANN (MODEL 1) USED IN THIS WORK.

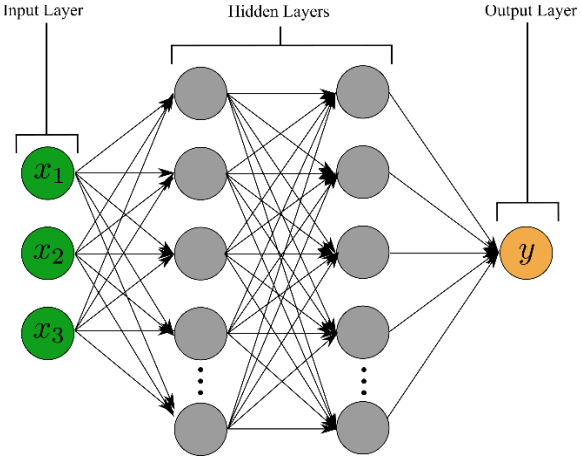

FIGURE 4: THE 2-LAYER ANN (MODEL 2) USED IN THIS WORK.

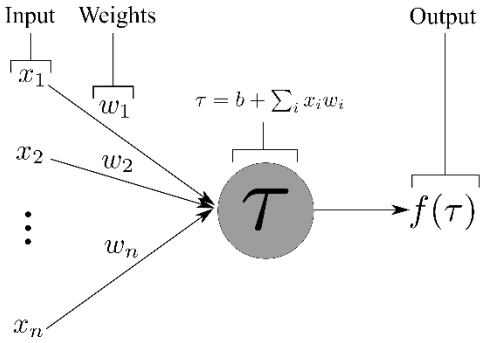

FIGURE 5: AN ANN NEURON SHOWING INPUTS, WEIGHTS, SUMMING, AND OUTPUT AS A FUNCTION OF THE WEIGHTED SUM.

A variety of activation functions have been used in ANNs. Three of the most common ones are the sigmoid, hyperbolic tangent ($\tanh(\tau)$), and rectified linear unit (ReLU) functions [38], given as

$$f_s(\tau) = \frac{1}{1+e^{-\tau}} \tag{5}$$

$$\tanh(\tau) = \frac{\sinh(\tau)}{\cosh(\tau)} = \frac{e^{2\tau}-1}{e^{2\tau}+1} \tag{6}$$

$$ReLU(\tau) = \max(0,\tau) \tag{7}$$

where $f_s(\tau)$ is the sigmoid function. These functions are shown in Fig. 6. They were also compared to the identity function $y = x$. Recently, the use of the ReLU function has become more common than traditional activation functions such as the hyperbolic tangent or sigmoid functions because it avoids the vanishing gradient problem [39]**.** A scoping study, not shown here, determined that the ReLU function was the most effective activation function for PV burst strength, although the hyperbolic tangent and sigmoid functions also performed well. As a result of this scoping study, and due to its common use in the literature, the ReLU function was selected for use in training the PV burst ANNs presented here.

3.3 Variable Normalization

Often in machine learning the raw data for different features can have order of magnitude differences in values. For example, with the PV burst data the D/t ratio ranges from 2.4 to 120 while the burst pressure ranges from 966 to 200000 psi. These severe differences in amplitude can make it difficult to train an effective ANN. To alleviate these differences the training data was normalized. Normalization involves scaling the entire data range so that the normalized data minimum becomes zero and the maximum becomes 1. This normalization, also known as the min-max scaler, is calculated for a given data point x as

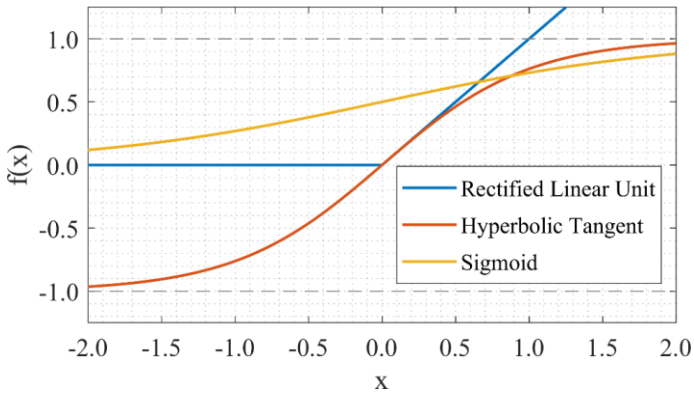

FIGURE 6: FREQUENTLY USED ACTIVATION FUNCTIONS FOR ANNS.

$$\hat{x} = \frac{x - x_{min}}{x_{max} - x_{min}} \quad (8)$$

where $\hat{x}$ is the normalized variable. A scoping study found that ANNs for PV burst performed much better when variable normalization was used, thus it was applied to each variable for all models presented here.

3.4 Cost Function

The root mean square error (RMSE) was used as a cost function to measure and compare different ANNs. The RMSE is calculated as

$$RMSE = \sqrt{\frac{1}{N}\sum_{n=1}^{N}\left(y_{n_{pred}} - y_{n_{act}}\right)^2} \quad (9)$$

where N is the total number of observations in the dataset, $y_{n_{pred}}$ is the nth value predicted by the ANN and $y_{n_{act}}$ is the nth actual value in the data set. Along with being used to compare networks, the RMSE gradient with respect to the weights is used by the backpropagation algorithm to update weight values during the training process.

3.5 Machine Learning Procedures

To train an artificial neural network the features chosen during the feature selection process, in this case D_o/D_i, σ_y, and σ_{uts} are normalized and then fed into the input layer. The algorithm then applied Eq. (4) to the input values to calculate the output value using the ReLU cost function. These values were passed as inputs to the next hidden layer for multiple layers, or for final processing in the output neurons, where the RMSE given in Eq. (9) is calculated. Once the RMSE is calculated, its gradient with respect to the weights and biases are calculated, and they are updated to reduce this error. This process is repeated over the number of epochs chosen, resulting in a fully trained ANN capable of predicting PV burst pressure.

4. RESULTS AND DISCUSSION

Matlab's machine learning toolbox was used for the development of the ANNs. This toolbox provides a simple easy to use interface, while also making machine learning functions available for more in depth ANN development. Using this feature makes it very easy to conduct parametric studies evaluating the performance of hundreds of different ANN's, something that would be more difficult in some other ANN applications. To develop high a performance ANN for model 1 and 2, several hyperparameters were investigated. Optimal parameters were also compared to the results of Matlab's optimizable neural network feature. For this ANN 20% of the data was randomly selected to be withheld for validation, while the other 80% was used for training.

4.1 Hyperparameter Selection

Three hyperparameter variables of interest, the number of neurons, the number of epochs (or iterations) and the regularization strength λ, were studied to find optimum values for these parameters. The number of epochs refers to how many times the backpropagation algorithm is implemented on a given data set to get effective bias b and weight w_i values. The regularization strength parameter λ determines the strength of the penalty for high amplitude weights w_i in the backpropagation algorithm, which helps prevent overfitting. For more information on regularization, see reference [39].

To determine optimum hyperparameters for models 1 and 2, the models were trained at different values ranging over a spectrum from 1 to 30 neurons per layer, 1 to 10,000 iterations for the epoch study and 1E-8 to 1E3 for the λ study. Because the performance of an ANN is dependent on the initial data randomly withheld for validation, for each number of neurons, value of λ, or number of epochs, the study reselected the data and retrained 100 different ANNs. The study then calculated the mean RMSE and found the minimum and maximum over these 100 models for each variable, to provide the possible range that the models could fall into.

The neuron study for both models 1 and 2 is shown in Figs. 7 and 8 respectively. The model 1 results shows that the mean RMSE and its range drops to mostly steady state values by 8 neurons. After this point, although the values do decline with increasing number of neurons, the decline is negligible. The model 2 results show that the mean RMSE and range have both settled to steady-state values by 10 neurons. Improvements beyond this point are negligible. As a result, 8 and 10 neurons were chosen respectively, resulting in a very low RMSE, while also keeping the model small to allow for quicker training time.

Figures 9 and 10 show the results of the epoch study for models 1 and 2 respectively. Figure 10 shows that for model 2, by 500 epochs the model range has reached a minimum, along with the RMSE. Figure 9 shows that this occurs sooner for model 1. However, for consistency between the two models, 500 epochs was selected for model 1 as well. It is interesting to note that model 1 reaches a minimum in both mean RMSE and range several hundred epochs before model 2. This is probably due to the reduced complexity of the model.

Figures 11 and 12 show plots of the mean RMSE in blue and model range in gray, as a function of number of epochs or λ value for models 1 and 2 respectively. Figure 11 shows that the mean RMSE and range for model 1 reach a minimum at $\lambda = 1E-5$. Figure 12 shows that the mean RMSE and range for model 2 reach a minimum at $\lambda = 1E-4$, an order of magnitude higher. The optimum results from all the studies presented in Figs. 7 – 12 are summarized in Table 1.

TABLE 1: OPTIMIZED HYPERPARAMETERS FOR THE ANN ALGORITHM.

Model	No. Neurons	No. Epochs	λ
1	8	500	1E-5
2	10	500	1E-4

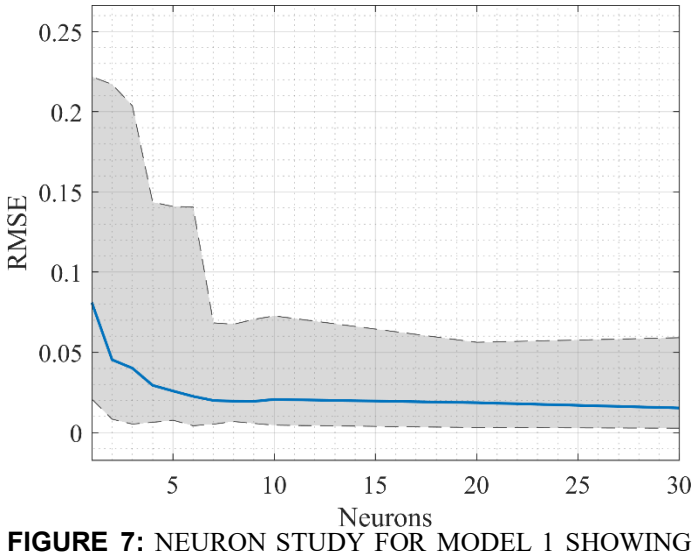

FIGURE 7: NEURON STUDY FOR MODEL 1 SHOWING THE MEAN RMSE OVER 100 MODELS IN BLUE AND THE MODEL RANGE IN GRAY.

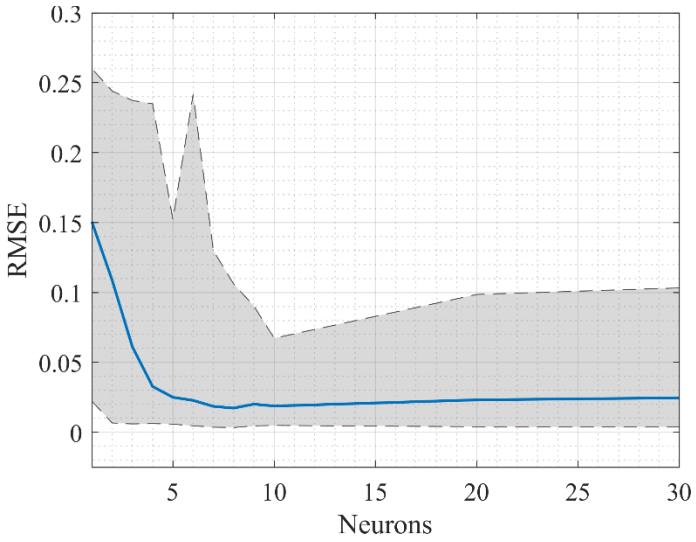

FIGURE 8: NEURON STUDY FOR MODEL 2 SHOWING THE MEAN RMSE OVER 100 MODELS IN BLUE AND THE MODEL RANGE IN GRAY.

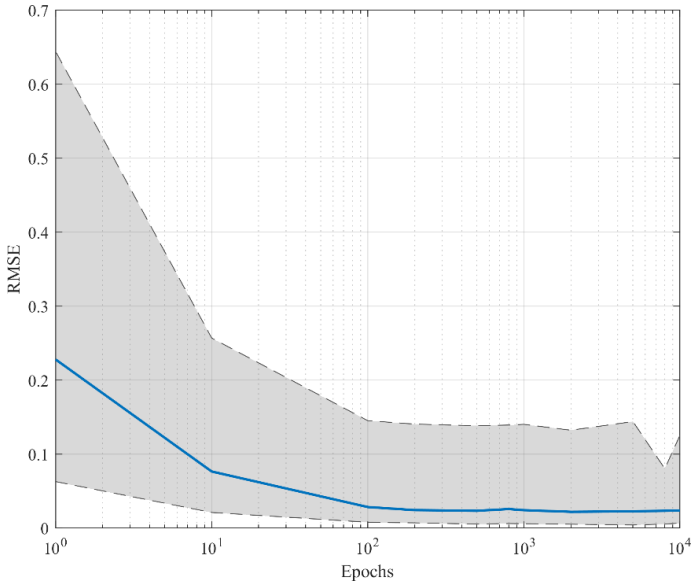

FIGURE 9: STUDY OF THE MEAN RMSE, IN BLUE, AND RANGE BARS, SHADED IN GRAY, AS A FUNCTION OF THE NUMBER OF EPOCHS, OVER 100 ANNS TRAINED ON RANDOMLY SELECTED DATA FROM THE DATASET FOR MODEL 1.

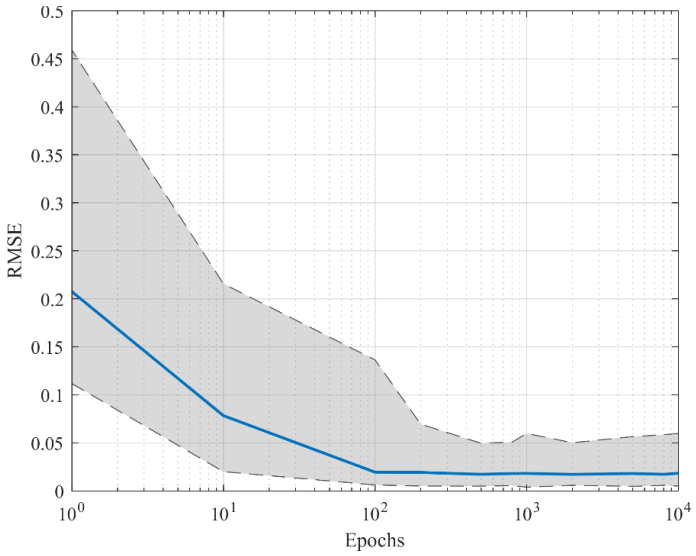

FIGURE 10: STUDY OF THE MEAN RMSE, IN BLUE, AND RANGE BARS, SHADED IN GRAY, AS A FUNCTION OF THE NUMBER OF EPOCHS, OVER 100 ANNS TRAINED ON RANDOMLY SELECTED DATA FROM THE DATASET FOR MODEL 2.

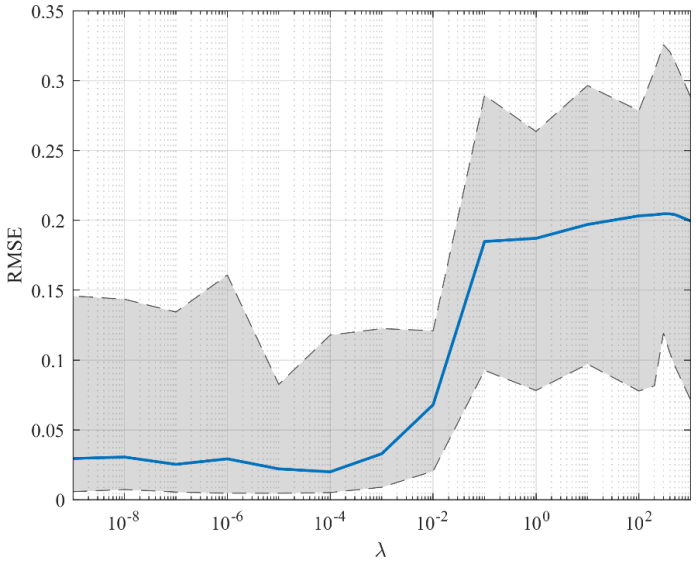

FIGURE 11: STUDY OF THE MEAN RMSE, IN BLUE, AND RANGE BARS, SHADED IN GRAY, AS A FUNCTION OF THE REGULARIZATION STRENGTH λ, OVER 100 ANNS TRAINED ON RANDOMLY SELECTED DATA FROM THE DATASET FOR MODEL 1.

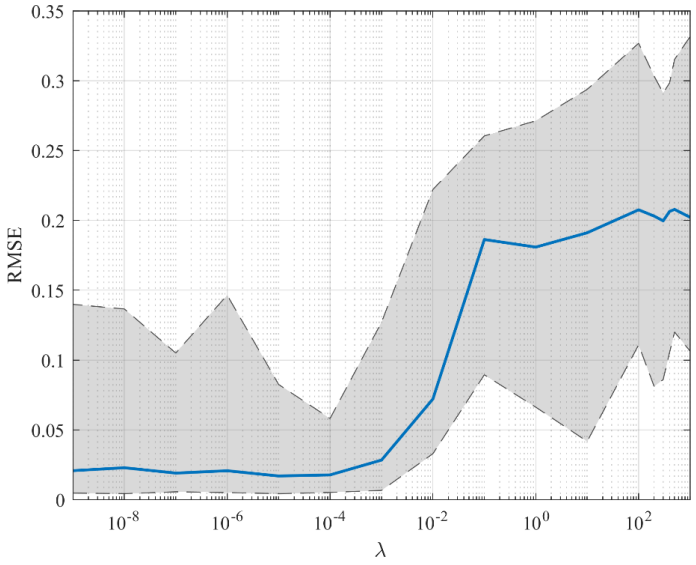

FIGURE 12: STUDY OF THE MEAN RMSE, IN BLUE, AND RANGE BARS, SHADED IN GRAY, AS A FUNCTION OF THE REGULARIZATION STRENGTH λ, OVER 100 ANNS TRAINED ON RANDOMLY SELECTED DATA FROM THE DATASET FOR MODEL 1.

4.2 Comparison of Model 1 and Model 2

Figure 13 shows a comparison of the predicted vs. actual burst pressure for the data shown in Fig. 1, for models 1 and 2, and the theoretical prediction using the Zhu-Leis thick-walled burst pressure prediction described in Eq. (1). Figure 14 shows a detailed view of the lower burst pressure range of Fig. 13 from 0 to 0.05, which encompasses all of the thin-walled PVs in the database ($D_o/t > 20$). These ANNs were trained using the optimal hyperparameters discussed in Secs. 3 and 4.1. The RMSE for each model is provided in Table 2.

The results in Figs. 13 and 14, and Table 2 show that both ANNs and Eq. (1) predict the burst pressure very close to what the actual burst pressure is, over the entire range of data. Both models predict lower burst pressures with higher accuracy, corresponding to thin-walled PVs, with only one outlier. In general, there is slightly larger error for high burst pressure data points corresponding to the thick-walled PV cases. This higher error is due to a lower amount of data covering a larger span of burst pressures and parameters, i.e., the database data density in the higher burst pressure range is lower. The results also show that, while in this case model 1 performs better than model 2, the difference is not significant, in both the final results shown in Fig. 13 and the hyperparameter studies presented in Figs. 7 – 12. These results suggest that a simple 1 layered ANN with optimal parameters will provide a good enough prediction of the pipeline burst pressure.

An alternative model, using an optimizable neural network, an option Matlab provides, was also examined. The optimizable neural networks tended to provide similar prediction to those presented here. However, the optimizer typically would find optimums using much larger numbers of neurons per hidden layer (more than 100), resulting in larger computation time with minimal improvements.

TABLE 2: COMPARISON OF RMSE VALUES OF THICK-WALLED BURST THOERY TO ANNS TRAINED USING OPTIMAL PARAMETERS.

	Model 1	Model 2	Eq. (1)
RMSE	0.0145	0.0164	0.0123

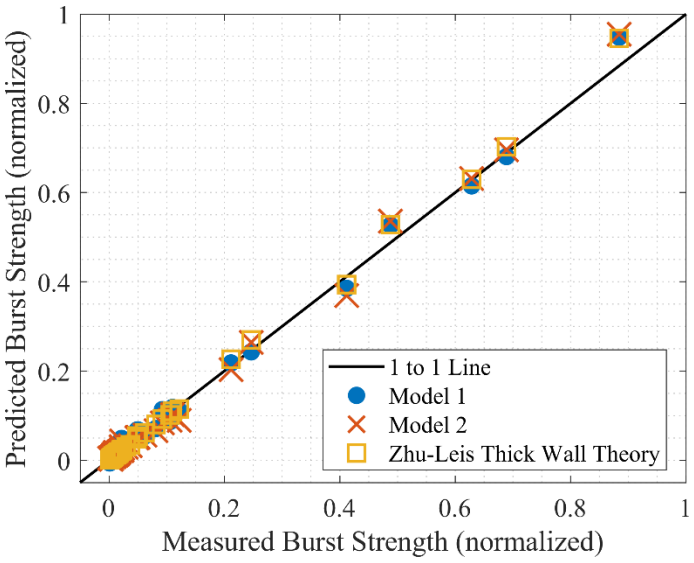

FIGURE 13: A COMPARISON OF THE MEASURED BURST PRESSURE VS. PREDICTED BURST PRESSURE FOR BOTH MODELS 1 AND 2.

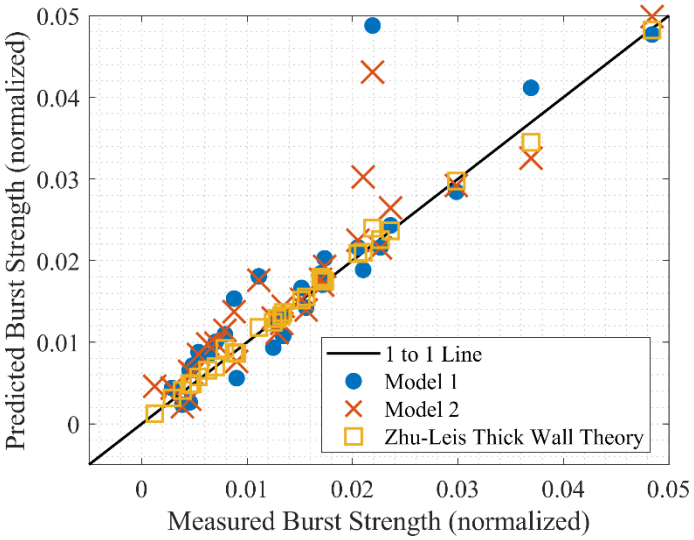

FIGURE 14: DETAIL VIEW OF THE 0 TO 0.15 X AND Y RANGE OF FIG. 13, SHOWING THE THIN-WALLED PV BURST RESULTS.

5. CONCLUSION

This work has developed 1 and 2 layered ANNs with 8 and 10 neurons per layer respectively, to predict the burst pressure of both thin and thick-walled linepipes and pressure vessels. The database used to train the ANNs combined data from multiple experimental sources in the literature, including both thin and thick-walled pipes, as well as data provided from FEA models. The hyperparameter study, which determined the performance of ANNs as a function of number of neurons, number of epochs, and the regularization parameter strength, based on a statistical study of the performance of a large number of ANNs, provided optimal hyperparameter values for training the most effective networks. The results showed that a minimum RMSE could be achieved using 500 epochs in each case, and a regularization value of 1E-5 for a 1 layered model and 1E-4 for a 2 layered model. Both the 1 and 2 layered models had very low RMSE values (RMSE < 0.02), suggesting that a very simple ANN can very accurately predict the burst pressure of linepipes. The primary results of this work include:

1. The first demonstration of ANN's that can predict the burst pressure for thin and thick-walled pressure vessels over a wide range of materials.
2. An ANN that was effectively trained using a combination of both experimental and numerically derived data.
3. Demonstration that a single hidden layer is sufficient to accurately predict the burst pressure of thin and thick-walled PVs.

The results of this work showed that the Zhu-Leis thick-walled PV burst theory is as accurate as the ANN's trained on experimental data. However, for more complex cases such as corrosion and defects, there currently are no accurate analytical theories. This work presents an important stepping-stone in developing ANNs that can accurately predict the burst pressure of PVs and linepipes with defects.

ACKNOWLEDGEMENTS

The authors are grateful for the financial support from the Department of Energy and its Laboratory Directed Research and Development (LDRD) program through the LDRD Project 2022-00077 at Savannah River National Laboratory.

REFERENCES

[1] M. Law and G. Bowie, "Prediction of failure strain and burst pressure in high yield-to-tensile strength ratio linepipe," *International Journal of Pressure Vessels and Piping,* vol. 84, 2007.

[2] T. Cristopher, B. Rama Sarma, P. Govindan Potti, B. Nageswara Rao and K. Sankarnarayanasamy, "A comparative study on failure of pressure estimations of unflawed cylindrical vessels," *International Journal of Pressure Vessels and Piping,* vol. 79, 2002.

[3] A. Nadai, Plasticity, McGraw-Hill, 1931.

[4] A. Nadai, Theory of flow and fracture of solids, New York: McGraw-Hill, 1950.

[5] X.-K. Zhu and B. N. Leis, "Theoretical and numerical predictions of burst pressure of pipelines," *Journal of Pressure Vessel Technology,* vol. 129, 2007.

[6] J. H. Faupel, "Yield and bursting characteristics of heavy-wall cylinders," *Transactions of the American Society of Mechanical Engineers,* vol. 78, no. 5, pp. 1031 - 1061, 1956.

[7] N. L. Svensson, "The bursting pressure of cylindrical and spherical vessels," *Journal of Applied Mechanics,* vol. 25, pp. 89-96, 1958.

[8] X.-K. Zhu, B. Wiersma, R. Sindelar and W. R. Johnson, "New strength theory and its application to determine burst pressure of thick-wall pressure vessels," in *Proceedings of the ASME 2022 Pressure Vessels & Piping Conference*, Las Vegas, NV, 2022.

[9] A. Karstensen, A. Smith and S. Smith, "Corrosion damage assessment and burst test validation of 8in X52 linepipe," in *Proceedings of ASME Pressure Vessel and Piping Conference*, Atlanta, GA, 2001.

[10] B. Fu and M. Kirkwood, "Determination of failure pressure of corroded linepipes using the nonlinear finite element method," in *Proceedings of the Second International Pipeline Technology Conference, Vol. II*, Ostend, Belgium, 1995.

[11] J. B. Choi, B. K. Goo, J. C. Kim, Y. J. Kim and W. S. Kim, "Development of limit load solutions for corroded gas piplines," *International Journal of Pressure Vessels and Piping,* vol. 80, 2003.

[12] K. J. Yeom, Y.-K. Lee, K. H. Oh and W. S. Kim, "Integrity assessment of a corroded API X70 pipe with a single defect by burst pressure analysis," *Engineering Failure Analysis,* vol. 57, 2015.

[13] H. C. Phan, A. S. Dhar and B. C. Mondal, "Revisiting burst pressure models for corroded pipelines," *Canadian Journal of Civil Engineering,* vol. 44, no. 7, 2017.
[14] N. Ihn and H. G. Nguyen, "Investigation of burst pressures in PWR primary pressure boundary components," *Nuclear Engineering and Technology,* vol. 48, pp. 236-245, 2016.
[15] C. J. Evans and T. F. Miller, "Failure prediction of pressure vessels using finite element analysis," *Journal of Pressure Vessel Technology,* vol. 137, p. 051206, 2015.
[16] D. H. Oh, J. Race, S. Oterkus and E. Chang, "A new methodology for the prediction of burst pressure for API 5L X grade flawless pipelines," *Ocean Engineering,* vol. 212, 2020.
[17] W. R. Johnson, X.-K. Zhu, R. Sindelar and B. Wiersma, "A parametric finite element study for determining burst strength of thin and thick-walled pressure vessels," *International Journal of Pressure Vessels and Piping,* vol. TBD, TBD.
[18] R. Silva, J. Guerreiro and A. Loula, "A study of pipe interacting corrosion defects using the FEM and neural networks," *Advances in Engineering Software,* vol. 38, 2007.
[19] A. Zolfaghari and M. Izadi, "Burst pressure prediction of cylindrical vessels using artificial neural network," *Journal of Pressure Vessel Technology,* vol. 142, 2020.
[20] D. Oh, J. Race, S. Oterkus and B. Koo, "Burst pressure prediction of API 5L X-grade dented pipelines using deep neural network," *Journal of Marine Science and Engineering,* vol. 8, no. 766, 2020.
[21] H. C. Phan and H. T. Duong, "Predicting burst pressure of defected pipeline with principal component analysis and adaptive neuro fuzzy inference system," *International Journal of Pressure Vessels and Piping,* vol. 189, 2021.
[22] H. C. Phan and A. S. Dhar, "Predicting pipeline burst pressures with machine learning models," *International Journal of Pressure Vessels and Piping,* vol. 191, 2021.
[23] W. Maxey, "Y/T significance in line pipe," in *Proceedings of the seventh symposium on line pipe research*, Houston TX, 1986.
[24] B. Chouchaoui, Evaluating the remaining strength of corroded pipelines, Departhment of Mechanical Engineering, University of Waterloo Canada, 1993.
[25] K. Amano, M. Matsuoka, T. Ishihara, K. Tanaka, T. Inoue, Y. Kawaguchi and M. Tsukamoto, "Significance of yield ratio limitation to plastic deformation of pipeline in high pressure proof test," in *Proceedings of the Seventh Symposium on Line Pipe Research*, Houston, TX, 1986.
[26] H. Hillenbrand, A. Liessem, G. Knauf, K. Niederhoff and J. Bauer, "Development of large-diameter pipe in grade X100," in *Proceedings of the Third International Conference of Pipeline Technology*, Brugge, Belgium, 2000.
[27] A. Liessem, M. Graef, G. Knauf and U. Marewski, "Influence of thermal treatment on mechanical properties of UOE linepipe," in *Proceedings of the Fourth International Conference of Pipeline Technology*, Ostend, Belgium, 2004.
[28] S. Okaguchi, H. Makino, M. Hamada, A. Yamamoto, T. Ikeda, I. Takeuchi, D. Fairchild, M. Macia, S. Papka, J. Stevens, C. Petersen, J. Koo, N. Bangaru and M. Luton, "Development and mechanical properties of X120 linepipe," *International Journal of Offshore Polar Engineering,* vol. 14, 2004.
[29] D. Mok, R. Pick, A. Glover and R. Hoff, "Bursting of line pipe with long external corrosion," *International Journal of Pressure Vessels and Piping,* vol. 46, no. 1, 1991.
[30] J. Kiefner, W. Maxey and A. Duffy, "The significance of the yield-to-ultimate strength ratio of line pipe materials. Summary report to Pipeline Research Committee," American Gas Association, 1971.
[31] S. Papka, J. Stevens, D. Macia, D. Fairchild and C. Petersen, "Full-size testing and analysis of X120 linepipe," *International Journal of Offshore Polar Engineering,* vol. 14, 2004.
[32] M. Law, G. Bowie and L. Fletcher, "Pipeline behaviour, the hydrostatic strength test, and failure strain," in *Proceedings of the 15th Conference of PRCI and EPRG Pipeline Conference*, Orlando FL, 2005.
[33] P. Paslay, E. Cernocky and R. Wink, "Burst pressure prediction on thin-walled, ductile tubulars subjected to axial load," in *Proceedings of Applied Technology Workshop on Risk Based Design of Well Cashing and Tubing*, Woodlands, TX, 1998.
[34] S. Zimmerman, S. Hohler and U. Marewski, "Modeling ultimate limit states on burst pressure and yielding of flawless pipes," in *Proceedings of the 16th Biennial Pipeline Research Joint Technical Meeting*, Canberra, Australia, 2007.
[35] X.-K. Zhu, "Strength criteria versus plastic flow criteria used in pressure vessel design design and analysis," *Journal of Pressure Vessel Technology,* vol. 138, 2016.
[36] X.-K. Zhu and B. N. Leis, "Average shear stress yield criterion and its application to plastic collapse analysis of pipelines," *International Journal of Pressure Vessels and Piping,* vol. 83, 2006.
[37] K. Fukushima, "Cognitron: a self-organizing multilayered neural network," *Biological Cybernetics,* vol. 20, 1975.
[38] C. Nwankpa, W. Ijomah, A. Gachagan and S. Marshall, "Activation functions: Comparison of trends in practice and research for deep learning," *arXiv preprint:1811.03378,* 2018.
[39] L. Melkumova and S. Shatskikh, "Comparing ridge and LASSO estimators for data analysis," *Procedia engineering,* vol. 201, pp. 746-755, 2017.

APPENDIX A: FINITE ELEMENT DERIVED PV BURST DATA

D_o (in)	Thickness t (in)	D_o/t	Material	Yield Stress (psi)	Engineering UTS (psi)	K (psi)	n	Burst Pressure (psi)
42	0.5	84	grade B	35677.94	60200	100135.3	0.192	1385.08
42	0.5	84	X52	52461.65	66700	95126.53	0.111	1618.971
42	0.5	84	X65	65627.32	77600	105200.6	0.089	1911.3
42	0.5	84	X70	70652.38	82700	111024.8	0.085	2043.059
42	0.5	84	X80	80903.51	90600	116425.9	0.068	2253.815
30	0.25	120	grade B	35677.94	60200	100135.3	0.192	965.603
30	0.25	120	X52	52461.65	66700	95126.53	0.111	1129.714
30	0.25	120	X65	65627.32	77600	105200.6	0.089	1333.066
30	0.25	120	X70	70652.38	82700	111024.8	0.085	1424.936
30	0.25	120	X80	80903.51	90600	116425.9	0.068	1571.907
30	0.5	60	grade B	35677.94	60200	100135.3	0.192	1948.807
30	0.5	60	X52	52461.65	66700	95126.53	0.111	2278.001
30	0.5	60	X65	65627.32	77600	105200.6	0.089	2689.657
30	0.5	60	X70	70652.38	82700	111024.8	0.085	2874.232
30	0.5	60	X80	80903.51	90600	116425.9	0.068	3171.63
30	0.75	40	grade B	35677.94	60200	100135.3	0.192	2949.557
30	0.75	40	X52	52461.65	66700	95126.53	0.111	3447.802
30	0.75	40	X65	65627.32	77600	105200.6	0.089	4069.46
30	0.75	40	X70	70652.38	82700	111024.8	0.085	4348.235
30	0.75	40	X80	80903.51	90600	116425.9	0.068	4800.269
24	0.25	96	grade B	35677.94	60200	100135.3	0.192	1209.834
24	0.25	96	X52	52461.65	66700	95126.53	0.111	1414.817
24	0.25	96	X65	65627.32	77600	105200.6	0.089	1670.237
24	0.25	96	X70	70652.38	82700	111024.8	0.085	1784.534
24	0.25	96	X80	80903.51	90600	116425.9	0.068	1969.429
24	0.5	48	grade B	35677.94	60200	100135.3	0.192	2447.103
24	0.5	48	X52	52461.65	66700	95126.53	0.111	2860.521
24	0.5	48	X65	65627.32	77600	105200.6	0.089	3377.029
24	0.5	48	X70	70652.38	82700	111024.8	0.085	3607.887
24	0.5	48	X80	80903.51	90600	116425.9	0.068	3982.265
24	1	24	grade B	35677.94	60200	100135.3	0.192	5004.949
24	1	24	X52	52461.65	66700	95126.53	0.111	5849.243
24	1	24	X65	65627.32	77600	105200.6	0.089	6905.101
24	1	24	X70	70652.38	82700	111024.8	0.085	7377.551
24	1	24	X80	80903.51	90600	116425.9	0.068	8148.59
16	0.5	32	grade B	35677.94	60200	100135.3	0.192	3711.283
16	0.5	32	X52	52461.65	66700	95126.53	0.111	4338.476
16	0.5	32	X65	65627.32	77600	105200.6	0.089	5121.019
16	0.5	32	X70	70652.38	82700	111024.8	0.085	5471.725

16	0.5	32	X80	80903.51	90600	116425.9	0.068	6041.389
16	0.75	21.33	grade B	35677.94	60200	100135.3	0.192	5662.478
16	0.75	21.33	X52	52461.65	66700	95126.53	0.111	6617.946
16	0.75	21.33	X65	65627.32	77600	105200.6	0.089	7812.825
16	0.75	21.33	X70	70652.38	82700	111024.8	0.085	8346.847
16	0.75	21.33	X80	80903.51	90600	116425.9	0.068	9220.088
8	0.5	16	grade B	35677.94	60200	100135.3	0.192	7683.312
8	0.5	16	X52	52461.65	66700	95126.53	0.111	8978.498
8	0.5	16	X65	65627.32	77600	105200.6	0.089	10600.61
8	0.5	16	X70	70652.38	82700	111024.8	0.085	11325.05
8	0.5	16	X80	80903.51	90600	116425.9	0.068	12511.83
8	0.75	10.67	grade B	35677.94	60200	100135.3	0.192	11956.94
8	0.75	10.67	X52	52461.65	66700	95126.53	0.111	13971.59
8	0.75	10.67	X65	65627.32	77600	105200.6	0.089	16493.93
8	0.75	10.67	X70	70652.38	82700	111024.8	0.085	17618.96
8	0.75	10.67	X80	80903.51	90600	116425.9	0.068	19473.28
8	1	8	grade B	35677.94	60200	100135.3	0.192	16586.19
8	1	8	X52	52461.65	66700	95126.53	0.111	19372.98
8	1	8	X65	65627.32	77600	105200.6	0.089	22871.1
8	1	8	X70	70652.38	82700	111024.8	0.085	24435.16
8	1	8	X80	80903.51	90600	116425.9	0.068	27002.81